Hindawi
Journal of Nanomaterials
Volume 2019, Article ID 6724018, 9 pages
https://doi.org/10.1155/2019/6724018

Research Article

Oxygen Vacancy Kinetics Mechanism of the Negative Forming-Free Process and Multilevel Resistance Based on Hafnium Oxide RRAM

Mingqun Qi,[1] Cuiping Guo,[1] and Meihan Zeng[2]

[1] *Department of Materials Science and Engineering, University of Science and Technology Beijing, Beijing 100083, China*
[2] *School of Mechanical Engineering, University of Science and Technology Beijing, Beijing 100083, China*

Correspondence should be addressed to Cuiping Guo; cpguo@ustb.edu.cn

Received 17 May 2018; Revised 10 November 2018; Accepted 24 January 2019; Published 20 March 2019

Academic Editor: Ilaria Fratoddi

Copyright © 2019 Mingqun Qi et al. This is an open access article distributed under the Creative Commons Attribution License, which permits unrestricted use, distribution, and reproduction in any medium, provided the original work is properly cited.

Switching between high resistance states and low resistance states in a resistive random access memory device mainly depends on the formation and fracture of conductive filaments. However, the randomness of the conductive filament growth and the potential breakdown of the large voltage in the forming process will lead to unstable resistive switching and memory performance. We studied the possible natural forming process of conductive filaments for intrinsic defects under the influence of top electrode material based on the structure of W/HfO_{2-x}/Pt. Such a simple device shows long retention time and great endurance cycles. The dendritic oxygen vacancy (V_O) conductive filament model was constructed, and the dynamic V_O migration under directional external bias was described according to the characteristic electrical performance. In addition, we also explored the relationship between the multilevel resistance and the evolution of a dendritic V_O conductive filament, signifying the potential application of multilevel storage in the future. Furthermore, a Ag/HfO_{2-x}/Ag selector was fabricated to assemble the memory device in wire connection which exhibits the potential of eliminating leaky current in the memory array. The connection also indicates that the fabrication process of the 1S1R structure can be simplified by using the same functional layer.

1. Introduction

With the advent of the big data era, the explosive amount of information requires researchers to constantly seek for memory such as high-speed operation, large on/off ratio, reliable switching endurance, long high-temperature lifetime, multivalue storage, and high device yield [1]. Based on these requirements, researchers worked on developing new storage and have achieved good results such as phase change memory (PCM) [2–4], ferroelectric random access memory (FRAM) [5–7], and flash memory [8–10]. As a candidate for next-generation memory storage, resistive random access memory (RRAM) has attracted more and more researchers' attention because it has the potential to achieve the excellent storage properties mentioned above [11–13]. Metal oxides of various properties have been used to study RRAM as materials because of full compatibility with the standard complementary metal oxide semiconductor (CMOS) process [14], such as TaO_x [15–17], Zr [18–20], ZnO_2 [21–23], TiO_2 [24–26], and HfO_{2-x} [27, 28]. In these materials, as an excellent storage medium, HfO_{2-x} has been the research focus. Complying with the CMOS process of the HfO_{2-x}, a film can be rapidly prepared [29] with less power consumption and good stability and reliability [30, 31]. HfO_{2-x} also shows excellent performance in the applications of band width [32] and resistance range [30]. The retention of the HfO_{2-x} system at high temperature [33] and low temperature [34] has also been verified. Chand et al. designed a structure of the Ti/Al_2O_3/TiO_2/TiN device by inserting an Al_2O_3 layer between the Ti top electrode and HfO_{2-x} layer and conducting high-temperature vacuum annealing and postmetal annealing treatments for achieving the thermal stability and reliability [33]. On the other hand, Fang et al. adopted a Pt/HfO_x/TiN structure to stabilize the performance of RRAM in low temperature [34]. Yoon et al. had designed a Pt/Ta_2O_5/HfO_{2-x}/Ti structure to stabilize the range of

resistance change in multilevel [30]. However, the reliable retention and stable multilevel resistance are still worth our improvement. In order to solve the physical mechanism of device operation, we need to stabilize low operating voltage [35], especially the large voltage which could not be reduced in the forming process the resistive switching [36]. In this study, we fabricated a W/HfO_{2-x}/Pt RRAM structure to investigate the effect of an oxytropic electrode on the distribution of oxygen vacancy (V_O) in a single layer HfO_{2-x} structure. The device shows great retention and endurance performance. In the negative sweeping process, the resistance of the device changes from a low resistance state (LRS) to a high resistance state (HRS) indicating the intrinsic formation of V_O conductive filaments (CFs) from bottom to top. In addition, the evolution model of V_O CFs is also constructed. For implementation of large-scale integration on a crossbar array, we also fabricated a selector with the structure of Ag/HfO_{2-x}/Ag, showing a decent selectivity in both positive and negative threshold switching. And we wire-connect the resistive memory with the selector in series, exhibiting the potential of alleviating the leaky current and simplifying the fabrication process. On this basis, such realization of multivalue storage and 1S1R (one selector and one resistive memory) unit performance provides ideas and suggestions for future application.

2. Experimental Section

2.1. Device Fabrication. The device was deposited by magnetron sputtering on a hot oxide silicon substrate with previously deposited ~120 nm Pt, served as bottom electrode (BE). During the sputtering process, the cavity vacuum was kept at 5.0×10^{-5} Pa. The radio frequency (RF) power supply was used to sputter the HfO_{2-x} ceramic target with the Ar flow rate of 6.6 sccm. After breaking the vacuum, the ~50 nm W top electrode (TE) was sputtered by direct-current (DC) power supply with the Ar flow rate of 5.5 sccm, using a mask to form circular TE patterns with a diameter of 500 μm. For the selector fabricated on the SiO_2/Si substrate, both TE and BE were Ag (~80 nm) and deposited by DC sputtering power supply with the Ar flow rate of 5.3 sccm. The HfO_{2-x} was deposited under the same parameters of fabricating HfO_{2-x} of the resistive memory device.

2.2. Device Characterization. The device structure was analyzed by the X-ray photoelectron spectroscopy (XPS) depth profiling. In the depth profile process, the sputtering rates of W and HfO_{2-x} were 4.24 nm/min and 4.00 nm/min, respectively. TE was stripped off ~30 nm at a large sputtering rate followed by conducting a lower sputtering rate at ~3.2 nm/min. Electrical characterization was conducted by the semiconductor parameter analyzer (Agilent B1500).

2.3. Results and Discussion. Figure 1(a) shows the structure of the W/HfO_{2-x}/Pt device. The binding force of Pt electrode and silicon substrate is relatively small. Before sputtering Pt electrode, in order to enhance the binding force of the film and the silicon substrate, we first sputter on the silicon substrate with titanium which has better binding force both with silicon substrate and Pt electrode. In the sputtering W electrode, we use a cover plate with a circular hole so that we can get multiple W/HfO_{2-x}/Pt devices at the same time. The chemical composition measurement obtained from the depth profile of the film using XPS is shown in Figure 1(b). The thicknesses of W and HfO_{2-x} are ~50 nm and ~30 nm, respectively. The thickness of the HfO_{2-x} function layer is the focus of our attention. Therefore, when it completely sputters to the Pt layer, it ends the depth profile process. Therefore, the relevant information of the Pt layer is not reflected in Figure 1(b). Since nuclear radiuses of the element are varying, the energies of O atoms and Hf atoms are different; it is not possible to ensure that the ratio of O atoms and Hf atoms sputtered is exactly 2 : 1, when the same Ar atoms are used to sputter HfO_2, as shown in Figure 1(b). According to the XPS results, the ratio of Hf and O is 1.87 : 1, i.e., the value of x in HfO_{2-x} is 0.13. The formation of oxygen vacancy is also one of the important reasons for the performance of this system.

Because of the absence of oxygen in HfO_{2-x}, we generally believe that the conductive mechanism of the system is the directional displacement of oxygen vacancy. Metal W has a strong affinity for oxygen atoms, which is one of the important reasons for using the W as the top electrode (TE) material. At the same time, the Pt as the bottom electrode (BE) has the less binding force with oxygen atom than W metal. The oxygen vacancies are much easier to be orientated or aligned spontaneously than that in other system. Thus, the natural oxygen vacancy conductive filaments (CFs) exist in the HfO_{2-x} film which results in the initial low resistant state (LRS).

The resistive switching (RS) characteristic of the W/HfO_{2-x}/Pt structure is shown in Figure 2(a). Each cycle starts with a negative voltage, sweeps back to the positive, and finally goes back to zero, i.e., $0\,V \rightarrow -3.5\,V \rightarrow 0\,V \rightarrow 3.5\,V \rightarrow 0\,V$. It should be noticed that the V_O's can accumulate spontaneously and form CFs with different connection strengths in the device. That means that the device can be switched by relatively low negative sweeping voltage rather than traditional large forming voltage to realize a forming-free process, and we can also modulate the ending voltage value appropriately during the negative sweeping process to prevent the device from failure effectively. In the endurance test, the set pulse is programed at 4 V/50 μs followed by read pulse 0.2 V/300 μs. The reset pulse is programed at −3.5 V/50 μs followed by the same read pulse. As shown in Figure 2(b), the on-off ratio of endurance can still be divided clearly after 10^5 cycles. A decent retention is demonstrated in Figure 2(c). At the reading voltage of 0.2 V, the LRS and the high resistance state (HRS) can be maintained for more than 10^6 s with a little shrinking on-off ratio at room temperature (RT). This may be due to the absorption of oxygen atoms by the device during testing in the atmosphere. Both endurance and retention performances exhibit the robust potential application of our device. Figure 2(d) shows statistical results of the SET voltages in a 100 DC cycling sweep process. In the wider range (1.38 V to 2.85 V), the mode of the switching voltage is 2.3 V which still belongs to the SET voltages.

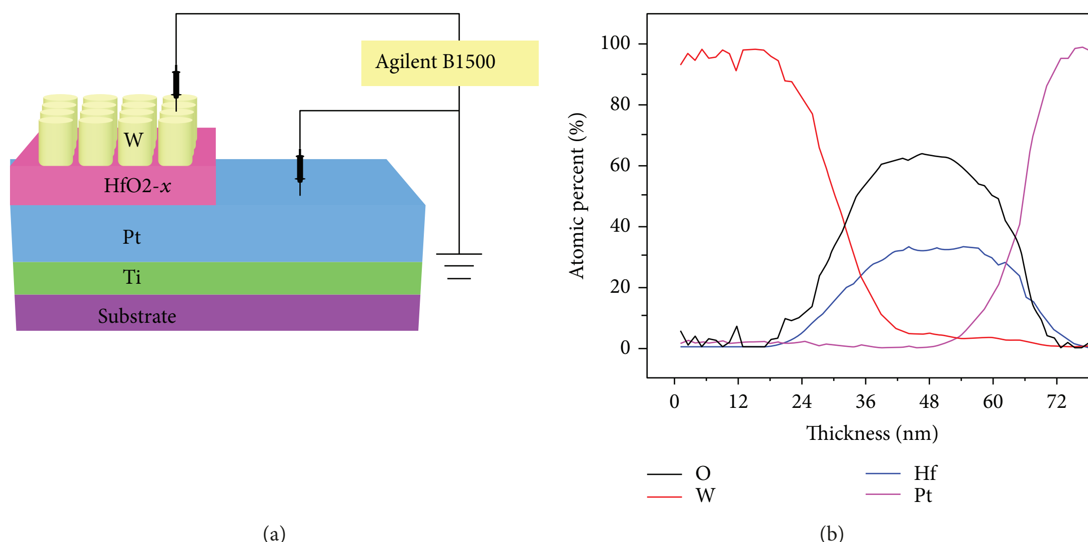

Figure 1: The structure and X-ray photoelectron spectroscopy (XPS) atomic percent of the device: (a) the structure of the W/HfO_{2-x}/Pt device and (b) the chemical composition measurement obtained from the depth profile of the film using XPS.

It is noticeable that the step-shape-like change of the conductance appears during both positive and negative sweep processes, implying the potential of adjustable multilevel storage. We believe that this resistance change is related to the multiple formation and fracture of CFs in the HfO_{2-x} functional layer. Next, the conductive mechanism of the W/HfO_{2-x}/Pt device is demonstrated in Figure 3. As shown in Figure 3(a), before the negative voltage is applied to the device, the LRS is spontaneously generated with the end of the device sputtering. Because metal W has a stronger binding force with oxygen than Pt, more oxygen vacancies will be accumulated at the BE. The result is that the concentration of oxygen vacancies near BE is greater than the oxygen vacancy concentration near TE. The concentration gradient of oxygen vacancy assists the formation of V_O CFs in the HfO_{2-x} functional layer. According to process I in Figure 2(a), the initial state of the device is in LRS. During the negative sweeping process, a mentioned step-shape-like current in the I-V curve at ~−1.5 V indicates the potential of multilevel storage. In addition, the V_O CFs are difficult to grow and be gathered in a regular shape like metal CFs, such as Ag [37] and Cu [38], due to the intrinsic amorphism in the as-deposited HfO_2 film [39]. Moreover, a few of hafnium oxide nanocrystallines are formed during the deposited process due to activated evaporation effects. As a result, dissociative V_O's will be distributed separately when they meet and impact with those few nanocrystallines and thus will connect each other in deviated directions rather than in just one direction [40]. In other hafnium oxide-based systems [41, 42], the phase of the nanoscale hafnium oxide film can be transformed from amorphous to a crystalline state by conducting an external electrical field, resulting in the emerging of grain boundaries that help distribution of V_O's along the boundaries and interfaces between amorphous and crystalline areas to some extent, i.e., the path of V_O's. It is therefore reasonable that a dendrite-like CF forms between the TE and the BE, as shown in Figure 3(a). When the negative voltage is relatively low (~−0.8 V), the V_O's cannot be activated to move for the relatively lower external input electrical field. With the negative voltage increasing, i.e., the input energy exceeds the activated energy of the V_O's, V_O's start moving to TE. Since the size of V_O's and binding strength between V_O's and bottom electrode (BE) are varying, parts of CFs will rupture under the negative electrical field so that the resistance of the device increases step by step, as shown in Figure 3(b). When the negative voltage increases further, the effect of thermochemical reaction on CFs also becomes more remarkable. Thus, most of the CFs are fused by joule heat, and the effect of the electrical field also assists that fusing simultaneously, as shown in Figure 3(c). In the process II of Figure 2(a), the current is approximately linear with the decrease of negative voltage. It suggests the final structure or shape of CFs in the HRS is hardly affected by the gradually decreasing electrical field so that resistance of the device can still maintain at the HRS. During the positive sweeping process with a relatively low voltage value, the V_O gradually migrates to BE, but the CFs have not extended significantly and connected completely so that the resistance of device still stays in the HRS, as shown in Figure 3(d), corresponding to process III in Figure 2(a). When the electric field force increases with the increasing of positive voltage, the V_O's migrate and stack to the preformed CF branches with the assistance of positive electrical field force, as shown in Figure 3(e). Therefore, the value of resistance decreases abruptly from HRS to LRS. Unlike Figure 3(a), the generation of this CFs is due to the effect of the electric field force. In this case, there should be more oxygen vacancies near the BE than that on the initial state. The voltage sweeps back from 3.5 V to 0 V in process IV in Figure 2(a), which makes more V_O's migrate to BE to offset the effect of partly ruptured CFs, contributing to keeping the shape of CFs in LRS. Such evolution model of V_O CFs in the functional film is verified by the subsequent modulating negative sweeping voltage value and positive compliance current (CC) tests.

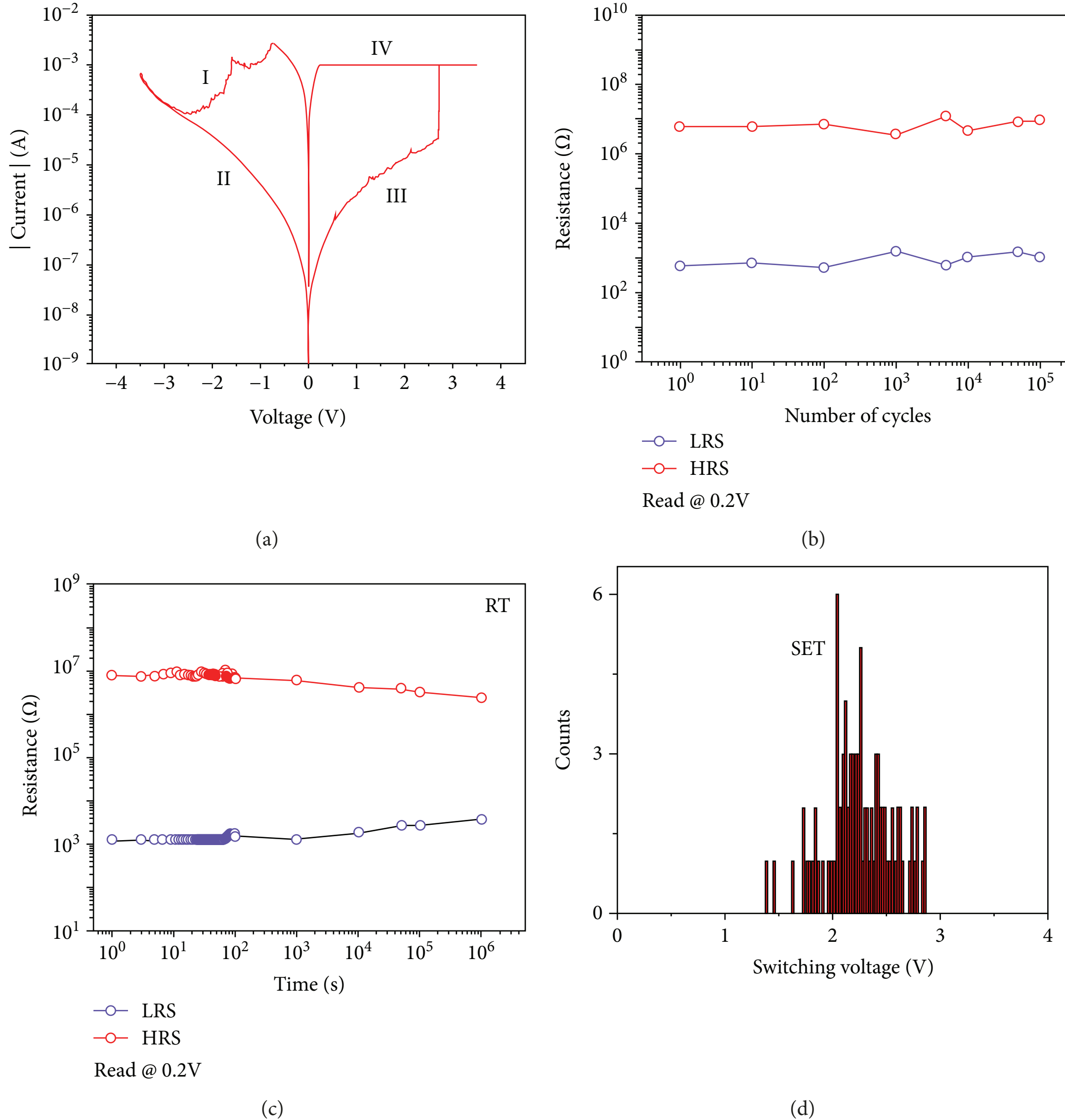

Figure 2: Electrical properties: (a) the resistive switching (RS) characteristic of the W/HfO_{2-x}/Pt structure and (b) pulse-tested endurance of the device. The set pulse is 4 V/50 μs followed by read pulse of 0.2 V/300 μs, and the reset pulse is −3.5 V/50 μs; (c) the retention test result after set and reset processes at room temperature; (d) statistical results of the SET voltages in the 100 DC cycling sweep process. Read pulse is 0.2 V/300 μs.

From the perspective of thermal dynamics of ion migrations, the dendritic CF model is still reasonable. This is because the migration of V_O under the electrical field predominates the conductive performance, which affects the growth and shape of CFs in great extent [43]. In the high ion mobility and low redox electrochemical metallization memristor, cations prefer to move toward the cathode, and CFs tend to grow from bottom to top for the high ion mobility. In the low redox process which results in limited supply of cations, the limited cations will be reduced at the tip of the existing CFs where the electrical field is enhanced, leading the formation of branch-shape CFs [44, 45]. In our system, the existence of a W electrode forms the channel for oxygen ions [46] and more likely to catch them, resulting in the inherent local concentration gradient of oxygen vacancy. So, the oxygen vacancy is much easier to decrease at the peak of preformed CFs and forms branch-shape CFs.

On the basis of that, we modulated the CC during the positive sweep process and maximal voltage value during the negative sweep process, respectively, to verify the existence of multilevel resistance or multilevel conductance in our device and the potential of storage application, as shown in Figures 4(a) and 4(b). The resistance of the device can be switched from HRS to LRS sharply at the CC of 100 μA, while the resistance of the device goes through a two-step resistive switching at the CC of 1 mA. Therefore, we believe that this phenomenon is a reconnection of CFs under the action of electric field force. At the same time, there is a new dendritic CF generation in the HfO_{2-x} functional layer [47]. Both the resistance under the CC of 1 mA and the resistance under

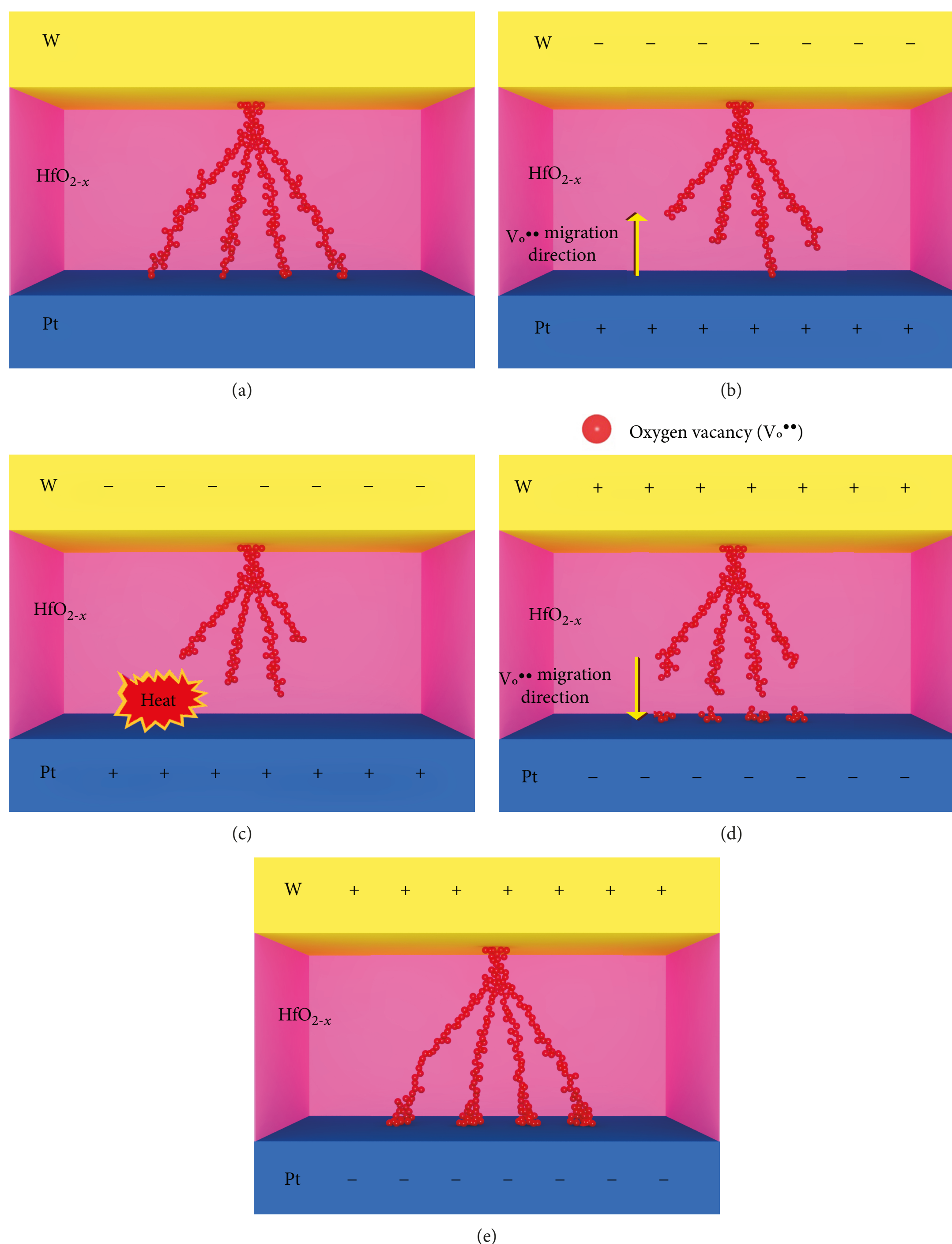

Figure 3: The demonstrated mechanism of RS performance change made in the W/HfO_{2-x}/Pt device: (a) a "dendrite" CF is formed between the TE and the BE, before applying the negative voltage to the device; (b) parts of CF rupture under the negative electrical field; (c) the remaining CFs are fused by generating joule heat; (d) the oxygen vacancy starts migrating to the bottom electrode, during the positive sweep process; (e) the oxygen vacancy connects with the preformed CF branches.

the CC of 100 μA can be sustained at LRS for a long period of time of 10^6 s. Resistances under different CCs have excellent stability and differentiation. In the same way, under the action of negative voltage of different sizes, the device also shows stable multiresistance performance, as shown in Figure 4(b). Different voltages will reconnect different numbers of disconnected CFs. We conduct different ending values of negative voltage to the device. When the negative voltage exceeds 3 V, the *I-V* curve presents the outgoing relationship. We believe that the device has reached the maximum resistance when the negative voltage is 3 V. Each resistance of HRS is stable and can be sustained for 10^6 s under negative voltages of 2 V, 2.5 V, and 3 V, respectively, as shown in Figure 4(d). After different negative ending

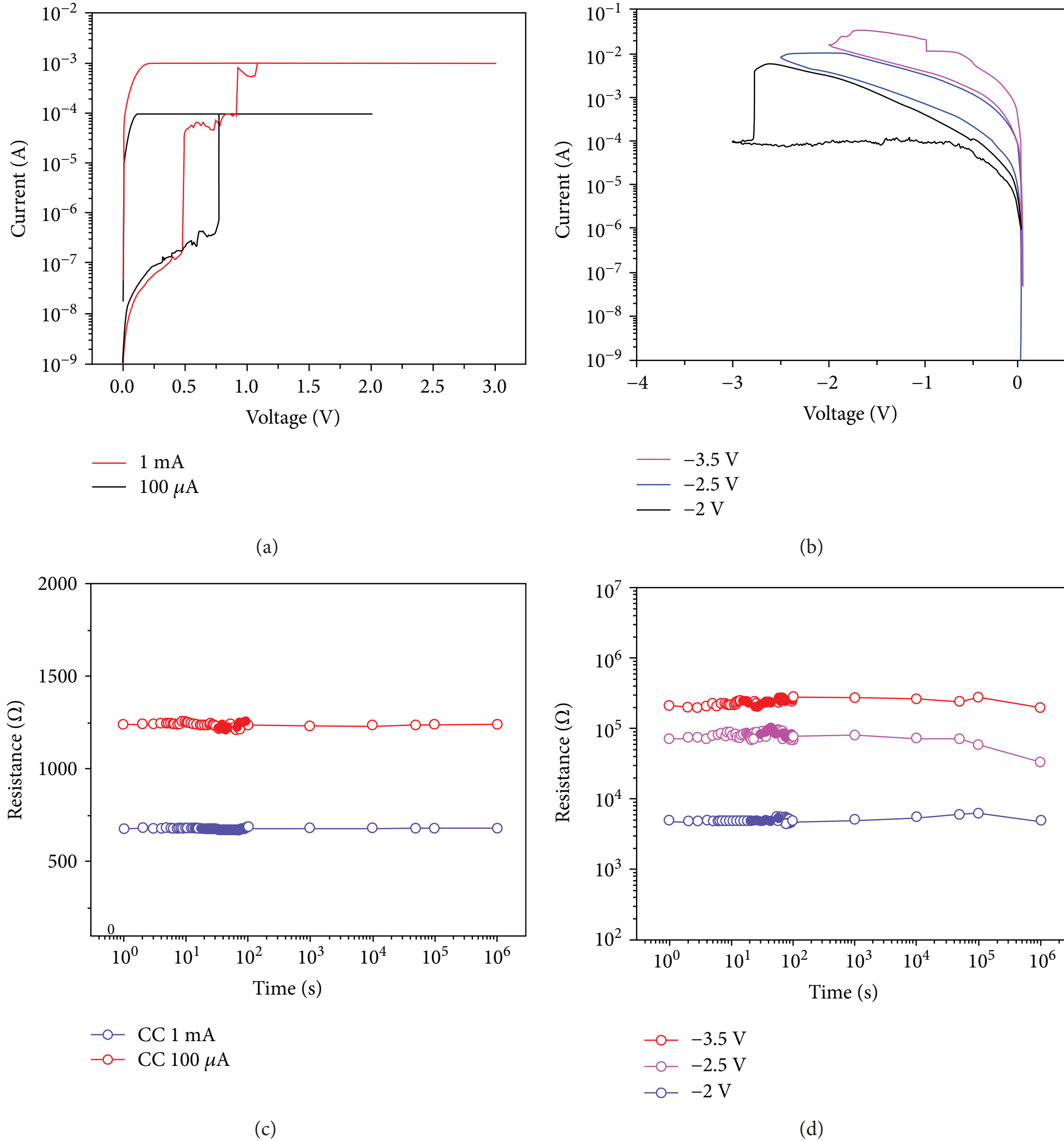

Figure 4: Electrical properties of the device in different voltages and compliance currents (CCs): (a) I-V curves of CC set at 1 mA and 100 μA, respectively; (b) I-V curves under different negative ending voltage values; (c) the retention test result after modulating the CC value; (d) the retention test result after modulating the negative ending voltage value (all retention tests are carried out at room temperature).

voltage sweeping processes, the device shows robust and fairly stable HRS. The phenomenon of multivalue resistance in different currents and voltages is one of the important properties of this device. This performance makes it possible for RRAM devices to be able to store more information without increasing their volume.

Furthermore, in order to put our device in large-scale integration like the crossbar array and neuromorphic computing, leaky current from nearby units, which can cause misreading during the operating period, is desired to be tackled [48–50]. A series of measurements, such as one diode and one resistive memory (1D1R) [48], one transistor and one resistive memory (1T1R) [49], and 1S1R [50], are designed to make great efforts on that problem. Unlike 1D1R and 1T1R whose sizes are relatively large compared with the resistive switching device, the 1S1R is the most promising structure for coping with the leaky current efficiently and compatibly. This is because the selector has higher selectivity and scalability than a diode or a transistor [50]. More importantly, the selector is flexible because it can stay at an extremely large value of resistance at low voltage before being turned on by large voltage, which can help eliminate leaky current that is usually low by that large resistance. Therefore, a decent selector with a structure of Ag/HfO_{2-x} (~30 nm)/Ag is fabricated and then connects the W/HfO_x/Pt device in series. Figure 5(a) shows a typical I-V characteristic of the selector, and an inset demonstrates a vertical structure of the selector. The voltage is applied in this

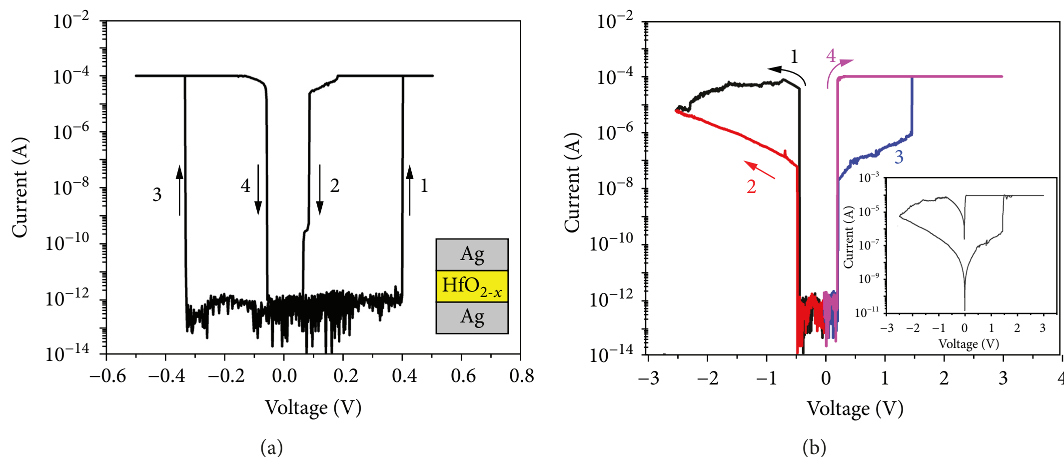

FIGURE 5: *I-V* characteristic of (a) a selector unit with the structure of Ag/HfO_{2-x}/Ag and (b) a 1S1R unit by connecting the W/HfO_{2-x}/Pt resistive memory (R) with the Ag/HfO_{2-x}/Ag selector (S) in series.

order: 0 V → 0.5 V → 0 V → −0.5 V → 0 V, and both directions of CC are 100 μA. When the positive voltage begins to sweep before ~0.4 V, the selector can keep stably at a large HRS. After the voltage sweeps over ~0.4 V, i.e., threshold voltage, it makes the resistance change sharply from HRS to LRS, i.e., ON-state. While the voltage sweeps back to 0 V, however, the device cannot hold LRS at low voltage ~0.1 V, thus making the device turn off, i.e., OFF-state. The *I-V* characteristic of the negative sweeping side is nearly the same as the positive one, and its ON-state voltage and OFF-state voltage are ~−0.34 V and ~−0.08 V, respectively. In addition, the selector also exhibits a large scalability of ~10^8, and thus, the operating current can be modulated extensively while that selector connects with a resistor in series.

The 1S1R structure is connected via an external circuit rather than depositing and stacking directly, i.e., the selector and our resistive switching device is fabricated separately and then assembled in a wire connection. The inset of Figure 5(b) displays the typical *I-V* curves of the W/HfO_{2-x}/Pt memory device. We testified the feasibility of that connection by four steps, as shown in Figure 5(b). In step 1, the selector turns to ON-state at ~0.3 V, and the memory then switches to LRS at ~1.5 V (blue line). Step 2 proves the fact that memory has already set to LRS and can keep at that state (magenta line). During step 3, i.e., the negative sweeping process, the selector turns on at ~0.4 V, and the memory resets gradually from ~−0.5 V to −2.5 V (black line). Step 4 verifies the memory is reset at HRS and can hold that state. This voltage sweep response reveals that the selector based on hafnium oxide is able to restrain the crosstalk issue in a large memory array which is also based on hafnium oxide, indicating the simplification of fabricating the 1S1R device by using the same functional layer.

3. Conclusions

In summary, we designed the structure of W/HfO_{2-x}/Pt RRAM and constructed the dendrite V_O CF model according to the step-like reset process under negative voltage sweeping. The device shows a negative forming-free process, great endurance and retention, and reliable multilevel resistance which can be modulated by controlling negative sweeping voltage or CC. The long retention of each resistance state verified dynamics of the dendrite V_O CF model. In addition, 1S1R in a wire connection also demonstrated a great potential for dealing with leaky current and was able to simplify the fabrication process of two devices (selector and resistive memory) due to no need of changing the functional layer. This W/HfO_{2-x}/Pt system provides a new way and guides for multivalue storage in the future investigation.

Data Availability

The data used to support the findings of this study are included within the article.

Conflicts of Interest

The authors declare that there is no conflict of interest regarding the publication of this paper.

Acknowledgments

This work was supported by the National Key R&D Program of China (Grant No. 2017YFB0702901) and National Natural Science Foundation of China (Grant No. U1602275).

References

[1] H.-S. P. Wong, H.-Y. Lee, S. Yu et al., “Metal–oxide RRAM,” *Proceedings of the IEEE*, vol. 100, no. 6, pp. 1951–1970, 2012.

[2] G. W. Burr, M. J. Breitwisch, M. Franceschini et al., “Phase change memory technology,” *Journal of Vacuum Science & Technology B, Nanotechnology and Microelectronics: Materials, Processing, Measurement, and Phenomena*, vol. 28, no. 2, pp. 223–262, 2010.

[3] S. Raoux, W. Wełnic, and D. Ielmini, “Phase change materials and their application to nonvolatile memories,” *Chemical Reviews*, vol. 110, no. 1, pp. 240–267, 2009.

[4] M. Salinga and M. Wuttig, “Phase-change memories on a diet,” *Science*, vol. 332, no. 6029, pp. 543-544, 2011.

[5] T. Kijima, T. Aoyama, H. Miyazawa et al., "Novel Si Codoped Pb(Zr,Ti,Nb)O_3 thin film for high-density ferroelectric random access memory," *Japanese Journal of Applied Physics*, vol. 44, no. 1A, pp. 267–274, 2005.

[6] K. R. Udayakumar, T. S. Moise, S. R. Summerfelt et al., "Full-bit functional, high-density 8 Mbit one transistor–one capacitor ferroelectric random access memory embedded within a low-power 130 nm logic process," *Japanese Journal of Applied Physics*, vol. 46, no. 4B, pp. 2180–2183, 2007.

[7] R. Guo, L. You, Y. Zhou et al., "Non-volatile memory based on the ferroelectric photovoltaic effect," *Nature Communications*, vol. 4, no. 1, p. 1990, 2013.

[8] S.-H. Lim and K.-H. Park, "An efficient NAND flash file system for flash memory storage," *IEEE Transactions on Computers*, vol. 55, no. 7, pp. 906–912, 2006.

[9] E. H. Nam, B. S. J. Kim, H. Eom, and S. L. Min, "Ozone (O_3): an out-of-order flash memory controller architecture," *IEEE Transactions on Computers*, vol. 60, no. 5, pp. 653–666, 2011.

[10] Y. Sun, H. Y. Yu, N. Singh, N. S. Shen, G. Q. Lo, and D. L. Kwong, "Multibit programmable flash memory realized on vertical Si nanowire channel," *IEEE Electron Device Letters*, vol. 31, no. 5, pp. 390–392, 2010.

[11] A. Chen, "Utilizing the variability of resistive random access memory to implement reconfigurable physical unclonable functions," *IEEE Electron Device Letters*, vol. 36, no. 2, pp. 138–140, 2015.

[12] J. Robertson and R. M. Wallace, "High-K materials and metal gates for CMOS applications," *Materials Science and Engineering: R: Reports*, vol. 88, no. 12, pp. 1–41, 2015.

[13] A. Sawa, "Resistive switching in transition metal oxides," *Materials Today*, vol. 11, no. 6, pp. 28–36, 2008.

[14] A. Abusleme, A. Dragone, G. Haller, and B. Murmann, "Mismatch of lateral field metal-oxide-metal capacitors in 180 nm CMOS process," *Electronics Letters*, vol. 48, no. 5, pp. 286-287, 2012.

[15] A. Wedig, M. Luebben, D. Y. Cho et al., "Nanoscale cation motion in TaO_x, HfO_x and TiO_x memristive systems," *Nature Nanotechnology*, vol. 11, no. 1, pp. 67–74, 2016.

[16] X. Tong, W. Wu, Z. Liu, X. A. Tran, H. Y. Yu, and Y.-C. Yeo, "Switching model of TaO_x-based nonpolar resistive random access memory," *Japanese Journal of Applied Physics*, vol. 52, no. 4S, 2013.

[17] W. Kim, B. Rösgen, T. Breuer et al., "Nonlinearity analysis of TaO_X redox-based RRAM," *Microelectronic Engineering*, vol. 154, pp. 38–41, 2016.

[18] D. Panda and T.-Y. Tseng, "Growth, dielectric properties, and memory device applications of ZrO_2 thin films," *Thin Solid Films*, vol. 531, no. 1, pp. 1–20, 2013.

[19] C.-Y. Lin, C.-Y. Wu, C.-Y. Wu et al., "Effect of top electrode material on resistive switching properties of ZrO_2 film memory devices," *IEEE Electron Device Letters*, vol. 28, no. 5, pp. 366–368, 2007.

[20] S.-Y. Wang, D.-Y. Lee, T.-Y. Huang, J.-W. Wu, and T.-Y. Tseng, "Controllable oxygen vacancies to enhance resistive switching performance in a ZrO_2-based RRAM with embedded Mo layer," *Nanotechnology*, vol. 21, no. 49, article 495201, 2010.

[21] N. Xu, B. Gao, L. F. Liu et al., "A unified physical model of switching behavior in oxide-based RRAM," in *2008 Symposium on VLSI Technology*, pp. 100-101, 2008.

[22] F. M. Simanjuntak, S. Chandrasekaran, B. Pattanayak, C. C. Lin, and T. Y. Tseng, "Peroxide induced volatile and non-volatile switching behavior in ZnO-based electrochemical metallization memory cell," *Nanotechnology*, vol. 28, no. 38, article 38LT02, 2017.

[23] X. Cao, X. Li, X. Gao et al., "All-ZnO-based transparent resistance random access memory device fully fabricated at room temperature," *Journal of Physics D: Applied Physics*, vol. 44, no. 25, article 255104, 2011.

[24] P. Bousoulas, I. Giannopoulos, P. Asenov, I. Karageorgiou, and D. Tsoukalas, "Experiments and simulation of multilevel resistive switching in forming free Ti/TiO_{2-x} RRAM devices," in *2017 Joint International EUROSOI Workshop and International Conference on Ultimate Integration on Silicon (EUROSOI-ULIS)*, pp. 172–175, 2017.

[25] W. Y. Chang, K. J. Cheng, J. M. Tsai et al., "Improvement of resistive switching characteristics in TiO_2 thin films with embedded Pt nanocrystals," *Applied Physics Letters*, vol. 95, no. 4, 2009.

[26] D. Carta, I. Salaoru, A. Khiat et al., "Investigation of the switching mechanism in TiO_2-based RRAM: a two-dimensional EDX approach," *Acs Applied Materials & Interfaces*, vol. 8, no. 30, article 19605, 19611 pages, 2016.

[27] D. Lee, Y. Sung, I. Lee, J. G. Kim, H. Sohn, and D. H. Ko, "Enhanced bipolar resistive switching of HfO_2 with a Ti interlayer," *Applied Physics A*, vol. 102, no. 4, pp. 997–1001, 2011.

[28] X. Sang, E. D. Grimley, T. Schenk, U. Schroeder, and J. M. LeBeau, "On the structural origins of ferroelectricity in HfO_2 thin films," *Applied Physics Letters*, vol. 106, no. 16, article 162905, 2015.

[29] M. Yang, E. P. Gusev, M. Ieong et al., "Performance dependence of CMOS on silicon substrate orientation for ultrathin oxynitride and HfO_2, gate dielectrics," *IEEE Electron Device Letters*, vol. 24, no. 5, pp. 339–341, 2003.

[30] J. H. Yoon, K. M. Kim, S. J. Song et al., "Pt/Ta_2O_5/HfO_{2-x}/Ti resistive switching memory competing with multilevel NAND flash," *Advanced Materials*, vol. 27, no. 25, pp. 3811–3816, 2015.

[31] F. M. Puglisi, L. Larcher, A. Padovani, and P. Pavan, "A complete statistical investigation of RTN in HfO_2-based RRAM in high resistive state," *IEEE Transactions on Electron Devices*, vol. 62, no. 8, pp. 2606–2613, 2015.

[32] K. B. Chung, M. H. Cho, U. Hwang et al., "Effects of postnitridation annealing on band gap and band offsets of nitrided Hf-silicate films," *Applied Physics Letters*, vol. 92, no. 2, 2008.

[33] U. Chand, K.-C. Huang, C.-Y. Huang, C.-H. Ho, C.-H. Lin, and T.-Y. Tseng, "Investigation of thermal stability and reliability of HfO_2 based resistive random access memory devices with cross-bar structure," *Journal of Applied Physics*, vol. 117, no. 18, article 184105, 2015.

[34] R. Fang, W. Chen, L. Gao, W. Yu, and S. Yu, "Low-temperature characteristics of HfO_x-based resistive random access memory," *IEEE Electron Device Letters*, vol. 36, no. 6, pp. 567–569, 2015.

[35] S. Ambrogio, S. Balatti, A. Cubeta, A. Calderoni, N. Ramaswamy, and D. Ielmini, "Statistical fluctuations in HfO_x resistive-switching memory: part I - set/reset variability," *IEEE Transactions on Electron Devices*, vol. 61, no. 8, pp. 2912–2919, 2014.

[36] P. Lorenzi, R. Rao, and F. Irrera, "Impact of forming pulse geometry and area scaling on forming kinetics and stability

of the low resistance state in HfO_2-based RRAM cells," in *2012 4th IEEE International Memory Workshop*, pp. 1–4, 2012.

[37] H. Sun, Q. Liu, C. Li et al., "Direct observation of conversion between threshold switching and memory switching induced by conductive filament morphology," *Advanced Functional Materials*, vol. 24, no. 36, pp. 5679–5686, 2014.

[38] W. Guan, M. Liu, S. Long, Q. Liu, and W. Wang, "On the resistive switching mechanisms of Cu/ZrO_2:Cu/Pt," *Applied Physics Letters*, vol. 93, no. 22, article 223506, 2008.

[39] H. Kim, P. C. Mcintyre, and K. C. Saraswat, "Effects of crystallization on the electrical properties of ultrathin HfO_2 dielectrics grown by atomic layer deposition," *Applied Physics Letters*, vol. 82, no. 1, pp. 106–108, 2003.

[40] B. Balamurugan and B. R. Mehta, "Optical and structural properties of nanocrystalline copper oxide thin films prepared by activated reactive evaporation," *Thin Solid Films*, vol. 396, no. 1-2, pp. 90–96, 2001.

[41] J. Yin, F. Zeng, Q. Wan et al., "Adaptive crystallite kinetics in homogenous bilayer oxide memristor for emulating diverse synaptic plasticity," *Advanced Functional Materials*, vol. 28, no. 19, article 1706927, 2018.

[42] J. Shang, W. Xue, Z. Ji et al., "Highly flexible resistive switching memory based on amorphous-nanocrystalline hafnium oxide films," *Nanoscale*, vol. 9, no. 21, pp. 7037–7046, 2017.

[43] J. Lee and W. D. Lu, "On-demand reconfiguration of nanomaterials: when electronics meets ionics," *Advanced Materials*, vol. 30, no. 1, 2018.

[44] M. H. Jang, R. Agarwal, P. Nukala et al., "Observing oxygen vacancy driven electroforming in Pt–TiO_2–Pt device via strong metal support interaction," *Nano Letters*, vol. 16, no. 4, pp. 2139–2144, 2016.

[45] S. Brivio, G. Tallarida, E. Cianci, and S. Spiga, "Formation and disruption of conductive filaments in a HfO_2/TiN structure," *Nanotechnology*, vol. 25, no. 38, article 385705, 2014.

[46] T. E. Madey, R. Stockbauer, J. F. van der Veen, and D. E. Eastman, "Angle-resolved photon-stimulated desorption of oxygen ions from a W(111) surface," *Physical Review Letters*, vol. 45, no. 3, pp. 187–190, 1980.

[47] Y. Yang and W. Lu, "Nanoscale resistive switching devices: mechanisms and modeling," *Nanoscale*, vol. 5, no. 21, article 10076, 10092 pages, 2013.

[48] C. H. Huang, J. S. Huang, S. M. Lin, W. Y. Chang, J. H. He, and Y. L. Chueh, "ZnO_{1-x} nanorod arrays/ZnO thin film bilayer structure: from homojunction diode and high-performance memristor to complementary 1D1R application," *ACS Nano*, vol. 6, no. 9, pp. 8407–8414, 2012.

[49] H. Liu, H. Lv, B. Yang et al., "Uniformity improvement in 1T1R RRAM with gate voltage ramp programming," *IEEE Electron Device Letters*, vol. 35, no. 12, pp. 1224–1226, 2014.

[50] R. Midya, Z. Wang, J. Zhang et al., "Anatomy of Ag/Hafnia-based selectors with 10^{10} nonlinearity," *Advanced Materials*, vol. 29, no. 12, article 1604457, 2017.

The Scientific World Journal
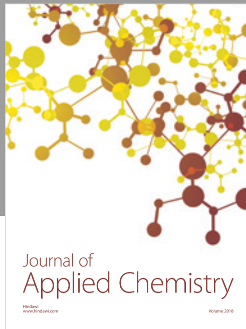
Journal of
Applied Chemistry
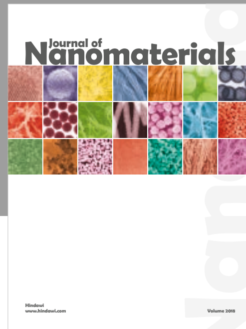
Journal of Nanomaterials
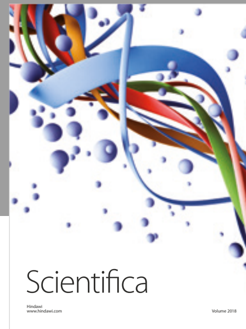
Scientifica

International Journal of
Polymer Science
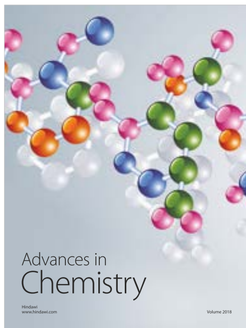
Advances in
Chemistry

Hindawi
Submit your manuscripts at
www.hindawi.com
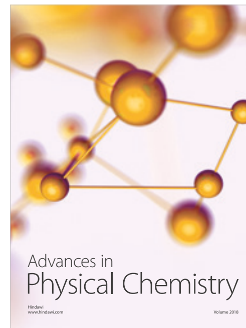
Advances in
Physical Chemistry

International Journal of
Analytical Chemistry
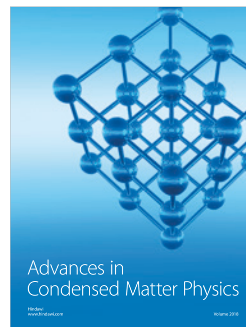
Advances in
Condensed Matter Physics

Journal of
Chemistry

International Journal of
Biomaterials
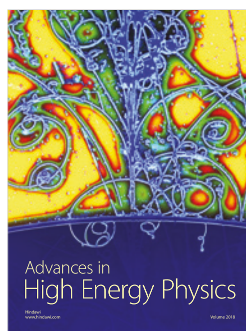
Advances in
High Energy Physics

Journal of
Engineering

Journal of
Nanotechnology

International Journal of
Corrosion

Journal of
Materials

BioMed
Research International

Advances in
Tribology
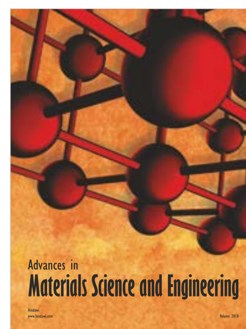
Advances in
Materials Science and Engineering